ISSN 1674-1056
http://cpb.iphy.ac.cn
http://iopscience.iop.org/cpb
中国物理 B
Chinese Physics
中国物理 Chinese Physics B

High-pressure-induced phase transition in cinchomeronic acid polycrystalline form-I

Ting-Ting Yan(颜婷婷), Dong-Yang Xi(喜冬阳), Jun-Hai Wang(王俊海), Xu-Feng Fan(樊旭峰), Ye Wan(万晔), Li-Xiu Zhang(张丽秀), Kai Wang(王凯)

Citation: Chin. Phys. B . 2019, 28(1): 016104. **doi:** 10.1088/1674-1056/28/1/016104
Journal homepage: http://cpb.iphy.ac.cn; http://iopscience.iop.org/cpb

What follows is a list of articles you may be interested in

Function of large-volume high-pressure apparatus at SECUF

Pinwen Zhu(朱品文), Qiang Tao(陶强), Lu Wang(王璐), Zhi He(何志), Tian Cui(崔田)
Chin. Phys. B . 2018, 27(7): 076103. **doi:** 10.1088/1674-1056/27/7/076103

Polycrystalline cubic boron nitride prepared with cubic-hexagonal boron nitride under high pressure and high temperature

Ming Yang(杨鸣), Zi-Li Kou(寇自力), Teng Liu(刘腾), Jing-Rui Lu(卢景瑞), Fang-Ming Liu(刘方明), Yin-Juan Liu(刘银娟), Lei Qi(戚磊), Wei Ding(丁未), Hong-Xia Gong(龚红霞), Xiao-Lin Ni(倪小林), Duan-Wei He(贺端威)
Chin. Phys. B . 2018, 27(5): 056105. **doi:** 10.1088/1674-1056/27/5/056105

Compression behavior and phase transition of β-Si_3N_4 under high pressure

Hong-xia Gong(龚红霞), Zi-li Kou(寇自力), Cong Fan(樊聪), Hao Liang(梁浩), Qi-ming Wang(王齐明), Lei-lei Zhang(张雷雷), Fang Peng(彭放), Ming Yang(杨鸣), Xiao-lin Ni(倪小林), Jing Liu(刘景)
Chin. Phys. B . 2018, 27(5): 056101. **doi:** 10.1088/1674-1056/27/5/056101

Density functional study on the pressure profile of the inhomogeneous fluid mixture

Yanshuang Kang(康艳霜), Yanmei Kang(康艳梅), Zongli Sun(孙宗利), Yushan Li(李玉山), Shanshan Tan(檀姗姗)
Chin. Phys. B . 2017, 26(8): 086101. **doi:** 10.1088/1674-1056/26/8/086101

Predicted novel insulating electride compound between alkali metals lithium and sodium under high pressure

Yang-Mei Chen(陈杨梅), Hua-Yun Geng(耿华运), Xiao-Zhen Yan(颜小珍), Zi-Wei Wang(王紫薇), Xiang-Rong Chen(陈向荣), Qiang Wu(吴强)
Chin. Phys. B . 2017, 26(5): 056102. **doi:** 10.1088/1674-1056/26/5/056102

High-pressure-induced phase transition in cinchomeronic acid polycrystalline form-I*

Ting-Ting Yan(颜婷婷)[1,†], Dong-Yang Xi(喜冬阳)[2], Jun-Hai Wang(王俊海)[3], Xu-Feng Fan(樊旭峰)[1], Ye Wan(万晔)[2], Li-Xiu Zhang(张丽秀)[3], and Kai Wang(王凯)[4]

[1] *School of Science, Shenyang Jianzhu University, Shenyang* 110168, *China*
[2] *School of Materials Science and Engineering, Shenyang Jianzhu University, Shenyang* 110168, *China*
[3] *Analysis and Detection Technology Research Center, Shenyang Jianzhu University, Shenyang* 110168, *China*
[4] *State Key Laboratory of Superhard Materials, Jilin University, Changchun* 130012, *China*

(Received 7 November 2018; revised manuscript received 8 November 2018; published online 30 December 2018)

Diamond anvil cells combined with Raman spectroscopy and angle-dispersive x-ray diffraction (ADXRD) were used to investigate the compression behavior of cinchomeronic acid ($C_7H_5NO_4$, CA), a hydrogen-bonded polymorphs. The compression of form-I at approximately 6.5 GPa caused an irreversible phase transition that produced the new polymorph form-III. Lattice and internal modes in the Raman spectra were analyzed to determine the modifications in the local environment of CA form-I molecules. The form-III was indexed and refined to a low-symmetry triclinic structure with space group $P1$. The mechanism for the phase transition involved the reconstructions in the hydrogen-bonded networks in CA form-I.

Keywords: phase transformations, pressure, vibrational spectroscopy, x-ray diffraction

PACS: 61.50.Ks, 82.80.Gk, 61.05.cp, 64.70.K **DOI:** 10.1088/1674-1056/28/1/016104

1. Introduction

Polymorphism is the phenomenon of the existence of more than one crystal structure for a given compound.[1] It was first found in arsenates and phosphates in 1822 by Mitscherlich.[2] Subsequently, Liebig and Wöhler studied benzamide as the earliest example of a polymorphic organic compound.[3] Thus far, the importance of polymorphism in the crystallization of organic compounds is widely recognized within the academic and industrial communities.[4–6] Different properties, such as hardness, density, solubility, and melting points[7,8] are particularly important for their behavior during processing and storage, as various manufacturing processes will be conducted before reaching the commercial available forms.[9] Therefore, the screening of polymorphs of a compound is of great interest and importance. Furthermore, the exploration of new polymorphs has become an issue for the industries in developing and marketing new products. The exploration of new polymorphs is not only an academic challenge but is also one of the most important goals in industry.

The use of high pressure for the compression of already known forms or high-pressure crystallization techniques has already been found to provide a new way of obtaining new polymorphs.[10] Hydrogen bonding, as an important and intensively studied noncovalent interaction, plays a crucial role in the crystal structures of organic crystals because of its specificity, directionality, and saturability.[11–13] Pressure can efficiently change the stabilities of crystal structures by modifying the geometry of the hydrogen bond, which can generate new structures and new properties.[14–16] Consequently, high-pressure technique can serve as a powerful tool to explore new polymorphs of hydrogen-bonded organic compounds. Numerous studies have been performed over the years to analyze high-pressure polymorphism in amino acid,[17,18] pharmaceuticals,[19–21] and energetic materials.[22,23] These studies indicate that the crystal structure can be modified, as well as completely changed, by adjusting the intermolecular hydrogen bonds at high pressures. Studies on high-pressure hydrogen-bonded organic polymorphic compounds can therefore clarify the nature of hydrogen bonds, as well as probe the polymorphism and pressure-induced phase transitions.

Cinchomeronic acid (CA; pyridine-3,4-dicarboxylic acid; $C_7H_5NO_4$) continues to attract the attention of chemists and biologists because of its special structures and properties.[24–28] CA is widely used in the construction of coordination networks, because its metal coordination modes allow for different architectures.[29,30] The presence of two polymorphs of CA has been reported in the PDF-2 since 1971. Forms-I and II can be prepared concomitantly from the recrystallization of form-II in ethanol/water solution at ambient conditions. Form-II transforms to form-I via a slurry conversion experiment. Both forms will decompose before melting form-I at 263 °C and form-II at 259 °C.

*Project supported by the National Natural Science Foundation of China (Grant Nos. 11604224, 51805336, and 11774120), the Open Project of State Key Laboratory of Superhard Materials of Jilin University, China (Grant No. 201708), the Natural Science Foundation of Liaoning Province, China (Grant No. 20180550861), the Education Department of Liaoning Province, China (Grant Nos. LJZ2016031 and LJZ2016030), and Shenyang Jianzhu University Discipline Content Education, China (Grant Nos. XKHY2-105 and XKHY2-101).

†Corresponding author. E-mail: yantt1120@163.com

© 2019 Chinese Physical Society and IOP Publishing Ltd

In the present study, we selected form-I as the model. Our approach has been to explore whether a new polymorph or a transformation between the two forms might occur at high pressures. Single-crystal x-ray diffraction analysis shows that form-I crystals at ambient pressures exhibit orthorhombic symmetry with space group $P2_12_12_1$.[28] The unit cell parameters are $a = 5.2864(4)$ Å, $b = 11.1966(8)$ Å, $c = 11.2293(8)$ Å, $V = 664.66(8)$ Å^3, and $Z = 4$. As shown in Fig. 1, the molecule takes the form of the zwitterion in the crystal with one acid hydrogen on the ring nitrogen. The carboxylic acid donates the hydrogen to the neighboring carboxylate forming an O_1–$H_{101}\cdots O_3$ hydrogen bond. This carboxylic group [$C_6(O_2)$–O_1–H_{101}] is involved in two quite short C_1–$H_1\cdots O_1$ and C_5–$H_5\cdots O_2$ hydrogen bonding interactions. The nitrogen atom in a pyridine ring participates in the formation of N_1–$H_{100}\cdots O_4$ hydrogen bond. Thus, each molecule forms four hydrogen bonds in a sort of tetrahedral coordination arrangement to give a three-dimensional complex network.

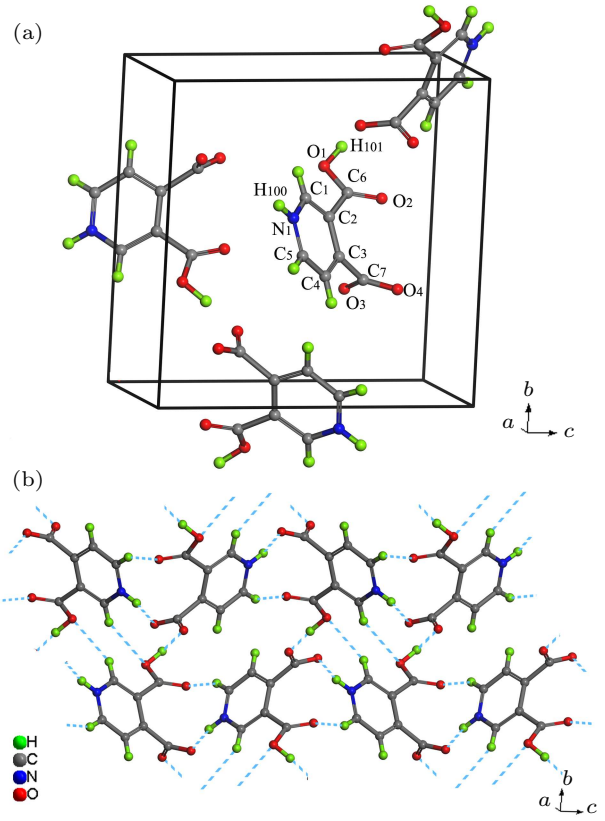


Fig. 1. Ambient pressure crystal structure (a) and hydrogen-bonded networks (b) of CA form-I.

2. Experimental setup

Commercially available pure monoclinic form-II of CA produced by Aldrich Company was used. The orthorhombic form-I with a rod-like habit was obtained from the recrystallization of form-II from ethanol/water solution. As shown in Fig. 2, the identity and crystallinity of form-I were confirmed by the conventional powder XRD because no diffraction signal was found from impurities in the pattern. The flawless crystals were selected and ground to powder with a grain size of approximately a few micrometers. The high-pressure experiments were performed with a polycrystalline form. A symmetric diamond anvil cell equipped with 400 μm culet diamonds was used to generate high pressure. A type 301 stainless steel gasket was preindented to 40 μm in thickness, and then a hole with a diameter of 130 μm was used as the sample chamber. A small ruby ball along with the polycrystalline sample was loaded into the chamber. Nitrogen was used as the pressure-transmitting medium to ensure hydrostatic pressure conditions,[31] and the pressure was determined by the ruby luminescence method.[32] All of the experiments were conducted at room temperature.

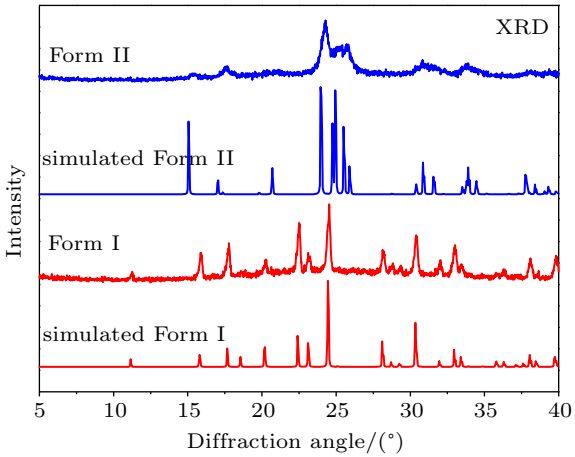


Fig. 2. The experimental and simulated powder XRD patterns of form-I and form-II.

High-pressure Raman spectra were recorded using an Acton SpectraPro 2500i spectrometer with a 532 nm laser excitation. Raman scattering was collected with backscattering configuration, and notch filters were utilized to get rid of the Rayleigh scattering. The resolution of the Raman system was ~ 1 cm^{-1}. High-pressure ADXRD experiments were conducted at the 4W2 high-pressure station of the Beijing Synchrotron Radiation Facility. Further analysis was performed with commercial Materials Studio 7.0 to gain accurate lattice parameters and possible space groups.

Ab initio calculations were performed with the norm-conserving pseudopotential plane-wave method implemented in the CASTEP code combined in the Materials Studio 7.0 program. The local density approximation exchange-correlation functional was used in the calculations. The geometry optimizations were performed by the BFGS algorithm. The k point has fine quality with 0.05 Å^{-1} separation.

3. Results and discussion

The point group symmetry of the CA form-I ($Z = 4$) is 222. The mechanical representation of this symmetry is

$$M = 51\mathrm{A} + 51\mathrm{B}_1 + 51\mathrm{B}_2 + 51\mathrm{B}_3,$$

of which three acoustic modes and 201 optic modes are found

$$\Gamma_{\text{acoustic}} = B_1 + B_2 + B_3,$$
$$\Gamma_{\text{optic}} = 51A + 50B_1 + 50B_2 + 50B_3.$$

Group theoretical classification of the 201 optical modes shows that the Raman-active modes belong to the $51A + 50B_1 + 50B_2 + 50B_3$ symmetry. Meanwhile, the $50B_1 + 50B_2 + 50B_3$ modes have infrared activity. Some Raman modes cannot be observed in our experiments probably because of particularly weak intensities.

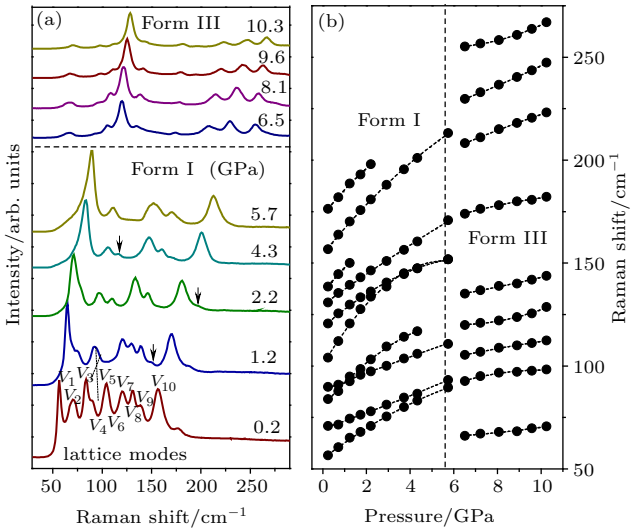


Fig. 3. (a) Raman spectra of CA form-I ranging from 30 cm^{-1} to 300 cm^{-1} as a function of pressure at room temperature; (b) corresponding frequency shifts. Nonlinear fits using a quadratic equation are performed for clarity.

The Raman modes of CA form-I were assigned based on the reported literature.[27] The evolution of Raman spectra ranging from 30 cm^{-1} to 300 cm^{-1} is shown in Fig. 3(a). The spectrum collected at ambient conditions includes 10 lattice Raman bands at 56, 70, 83, 89, 104, 120, 130, 139, 156, and 175 cm^{-1} (with the symbols ν_1–ν_{10}). Lattice modes in Raman scattering were correlated with collective motions of atoms in unit cell and widely adopted as evidence for crystal symmetrical change. Intermolecular hydrogen bonds (O–H···O, N–H···O, and C–H···O) play a key role in crystalline CA form-I; hence most of the lattice modes are involved in the hydrogen-bond vibrations. With increasing pressure, modes ν_3 and ν_4 overlap and cross each other by virtue of different shift rates. Then mode ν_3 loses its intensity and vanishes into the scattering background. Modes ν_8 and ν_{10} become too weak to be detected above 1.2 and 2.2 GPa, respectively. Mode ν_2 shifts to the margin of mode ν_1, and modes ν_5 and ν_6 merge together at 4.3 GPa. The spectral shape of the lattice modes noticeably changes at 6.5 GPa, indicating the transition from form-I to form-III. Moreover, there is no considerable broadening for the Raman peaks under compression. The FWHM (full width at half maximum) of the peaks support the phase transition. The original 10 vibrational modes absolutely lose their intensities with the appearance of nine new Raman peaks. The nine lattice modes in form-III keep their initial distribution in position and intensity without any discontinuous change up to 10.3 GPa, implying the stability of form-III up to the highest pressure of our experiment.

The pressure-induced frequency shifts of the lattice modes are depicted in Fig. 3(b). All the Raman peaks exhibit a substantial blue shift. The blue shift is caused by the reduced distances of adjacent molecules and increased intermolecular interactions.[33,34] An obvious discontinuity in shift rates is observed at 6.5 GPa, indicating the phase transition to form-III. The changes in the lattice Raman modes directly reveal the existence of new polymorph form-III at 6.5 GPa.

Raman spectra of CA form-I ranging from 300 cm^{-1} to 1800 cm^{-1} are illustrated in Fig. 4. The Raman peaks in this region were assigned to the internal framework modes. Compared with lattice modes, internal modes are more sensitive to pressure and can provide information on the chemical environment that surrounds a specific group. The simultaneous variations in internal modes confirm the occurrence of pressure-induced phase transition. At 6.5 GPa, some original modes disappear and new Raman modes emerge. The modes related to the pyridine ring skeleton, including CCCN torsion, CCCC torsion, CCN in-plane bending, CN stretching, CNH in-plane bending, CCH in-plane bending, CC ring stretching modes, show considerable changes during the phase transition. This result is because the increased pressure causes π–π stacking interaction to enhance, ultimately resulting in the rotations and distortions of the pyridine ring. Furthermore, the C–O stretching mode at 1120 cm^{-1} shifts to high frequency as a function of pressure, as shown in Fig. 4(b). The blue shift reflects that the N_1–H_{100}···O_4–C_7 hydrogen bonds in CA form-I are strong and continue to be strengthened with elevating pressure.[35,36] For weak- or moderate-strength hydrogen bonds, pressure can decrease the distance between H and O atoms. The enhanced electrostatic attraction should lengthen the C–O distance, resulting in the red shift of C–O stretching mode. However, for strong-strength hydrogen bonds, the shortened C–O distance displays blue shift. Similarly, the blue shift of the C–O stretching mode at 1383 cm^{-1} is due to the strong C_1–H_1···O_1–C_6 hydrogen bonds. Peak positions of the υC–O modes at 1120 cm^{-1} and 1383 cm^{-1} are shown in Table S1 in the Supplementary Material. It is noteworthy that the significantly enhanced Raman intensity of the υCO mode at 1383 cm^{-1} and the new υC=O mode marked by an asterisk in CA form-III. According to the Rietveld refinement result that will be discussed later, the C_1–H_1···O_1–C_6 hydrogen bonds are broken at high pressure, causing the enhanced Raman intensity of the υCO mode. Meanwhile, the new υC=O mode arises from new C_4–H_4···O_3=C_7 hydrogen bonds that exist in the form-III. Moreover, the abrupt changes with respect to C–COOH stretching, CCO in-plane bending, O–H out of plane bending, COO in-plane bending, CCCO torsion, CCOO torsion, COH

in-plane bending, CNH in-plane bending, CCH in-plane bending modes at 6.5 GPa suggest that the N–H···O and O–H···O hydrogen bonds evolve into a distorted state.

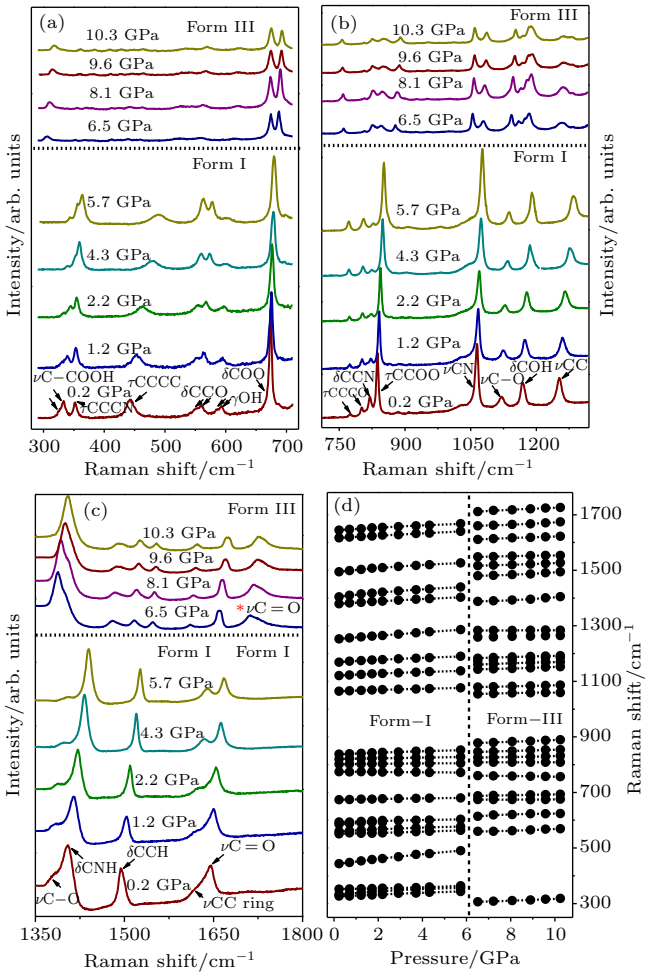


Fig. 4. Evolution of Raman spectra at high pressures in the regions of (a) 300–710 cm^{-1}, (b) 710–1320 cm^{-1}, (c) 1350–1800 cm^{-1}, and (d) corresponding frequency shifts. υ, stretching; τ, torsion; δ, in-plane bending; γ, out of plane bending.

The pressure dependence of corresponding internal modes is illustrated in Fig. 4(d). An obvious discontinuity is observed at ~ 6 GPa. This discontinuity is consistent with the proposed phase transition. All of the observed internal modes continuously present blue shifts arising from the contraction of covalent bond distances and the increase of corresponding effective force constants on increasing pressure. On the basis of the internal mode behavior, the molecular conformation, local environment around molecules, and hydrogen bonds in the CA form-I crystal dramatically change during phase transition. Furthermore, according to the frequency shifts of these internal modes, Grüneisen parameter has been calculated and analyzed, revealing the two different pressure regimes.

The phonon dispersion under pressure is described in terms of the Grüneisen parameter γ_i of the mode defined as

$$\gamma_i = -\frac{\partial \ln w_i}{\partial \ln V} = \frac{1}{\beta w_i}\frac{\partial w_i}{\partial P} = \frac{B}{w_i}\frac{\partial w_i}{\partial P},$$

where V is the unit cell volume of the crystal, ω_i is the phonon wavenumber, β is the isothermal compressibility, and P is the inducing pressure. The dimensionless quantity γ_i is obtained from the measured pressure dependence of the peak position ω_i and the isothermal compressibility value β, proportional to the inverse of the bulk modulus:

$$\beta = -\frac{1}{V}\left(\frac{\partial V}{\partial \rho}\right)_{\mathrm{T}} = -\frac{1}{B}.$$

A linear behavior was observed between ω and P. The data were therefore fitted using the least-squares technique. Values found for the Raman frequencies ω_i, the slope $\mathrm{d}\omega_i/\mathrm{d}P$, and the Grüneisen parameters are reported in Table S2 (Supplementary Material). As shown in Table S2, we observe only positive values for Grüneisen parameters. This means an increase of all vibrational modes with compression. Moreover, above ~ 6 GPa, the pressure dependence of the peak position shows a different dependence, as expressed by the calculated Grüneisen parameters, implying the phase transition from form-I to form-III. The parameters in the 6.6–10.3 GPa range are smaller than those in the 0–6 GPa range, indicating that vibrational bonding is more difficult to compress in the high pressure range.

The evolution of the C–H stretching region and their pressure dependence are summarized in Fig. 5, while the descriptors of hydrogen bonds, that is O–H stretching (3300–3500 cm^{-1}) and N–H stretching (3200–3300 cm^{-1}) modes cannot be detected in Raman experiments due to particularly weak intensities. The band at 3090 cm^{-1} was assigned to C–H symmetric stretching vibration, whereas the band at 3120 cm^{-1} was identified as C–H asymmetric stretching vibration. The blue shifts of the two modes are in accordance with the strong-strength C–H···O hydrogen bonds in CA form-I. At 6.5 GPa, the positions of the two modes present significant discontinuous changes. The combination of the evolutions of C–H stretching and CCH in-plane bending modes conclude that the C–H···O hydrogen bonds reconstruct with the application of pressure.

To gain further insight into the high-pressure behavior of hydrogen bonding, we have performed *ab initio* calculations using the pseudopotential plane-wave methods based on density functional theory. The calculated pressure-induced changes in the bond distances are shown in Table 1. From our calculations, the D–H bond length (D means donor) was shortened with increasing pressure, which is consistent with the blue shifts of the C–H stretching vibrations in Raman spectra. Meanwhile, the C–O bonds are also shortened with the application of pressure, implying the C–O stretching modes shifting to high frequency with pressure.

Table 1. *Ab initio* calculated changes in bond lengths (Å). Negative values indicate shortening.

Pressure/GPa	N_1–H_{100}···O_4–C_7		C_1–H_1···O_1–C_6		O_1–H_{101}···O_3=C_7		C_5–H_5···O_2=C_6	
	Δr(N–H)	Δr(O–C)	Δr(C–H)	Δr(O–C)	Δr(O–H)	Δr(O=C)	Δr(C–H)	Δr(O=C)
1	−0.004	−0.003	−0.007	−0.005	−0.006	−0.003	−0.008	−0.002
2	−0.006	−0.005	−0.012	−0.006	−0.011	−0.005	−0.013	−0.004
3	−0.007	−0.008	−0.018	−0.008	−0.013	−0.007	−0.021	−0.005
4	−0.010	−0.011	−0.022	−0.009	−0.015	−0.010	−0.026	−0.007
5	−0.012	−0.012	−0.029	−0.012	−0.018	−0.011	−0.031	−0.010
6	−0.013	−0.013	−0.032	−0.014	−0.019	−0.012	−0.038	−0.011

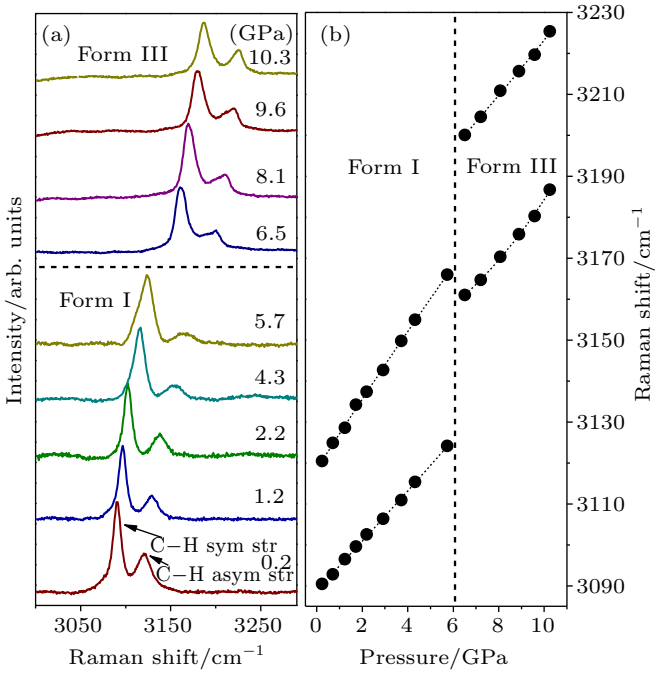


Fig. 5. (a) Evolution of Raman spectra of CA form-I in the C–H stretching region at different pressures; (b) frequency shifts of the two C–H stretching modes.

To confirm the pressure-induced phase transition and provide straightforward information about structural properties, high-pressure ADXRD experiments for CA form-I were conducted. The pressure-dependent variations in the ADXRD patterns are illustrated in Fig. 6(a). All the diffraction peaks of the CA form-I crystals shift to high angles upon compression, which suggests the reduction in the volume and intermolecular distance. Some new diffraction peaks marked by asterisks are observed at 6.6 GPa and gains in intensity gradually. Meanwhile, the peak marked with the down arrow cannot be detected anymore. The abrupt changes in the ADXRD patterns verify that CA form-I undergoes a pressure-induced phase transitions at around 6.5 GPa, which are similar to those of Raman investigations. More importantly, form-III can be retrieved on complete release of pressure. This irreversibility provides new insight in preparing new polymorphs using a high-pressure technique. Figure 6(b) shows the result of the Rietveld refinement of the released pattern based on the rigid body approximation. It is proposed that form-III possesses triclinic $P1$ symmetry, and the indexed lattice constants are $a = 6.921(2)$ Å, $b = 8.888(6)$ Å, $c = 13.759(9)$ Å, $\alpha = 132.33(0)°$, $\beta = 85.104(1)°$, $\gamma = 111.38(7)°$, $V = 566.70(6)$ Å^3, and $Z = 4$. This symmetry lowering through the phase transition is also reflected by the mode splittings in the Raman spectra.

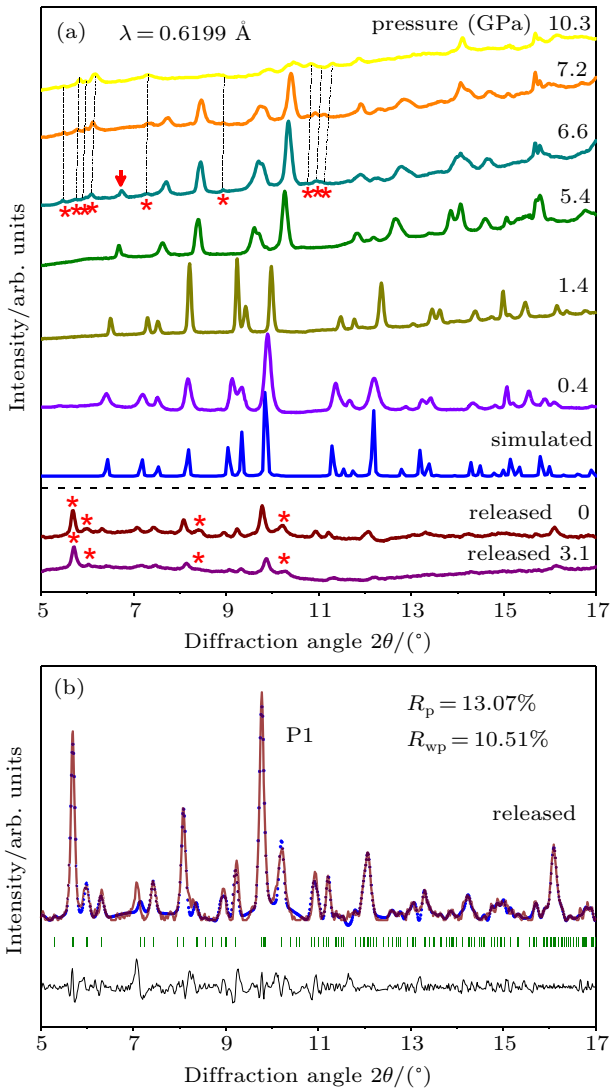


Fig. 6. (a) Representative ADXRD patterns of CA form-I at different pressures; (b) Rietveld refinement of form-III with respect to the pattern after complete release of pressure. Red, blue, and black lines represent experimental, calculated, and residual patterns, respectively.

The pressure dependences of the lattice parameters and unit cell volume are illustrated in Fig. 7. The volume (V) as a function of pressure (P) for the two forms was fit to a third-order Birch–Murnaghan equation of state

$$P(V) = \frac{3K_0}{2}\left[\left(\frac{V_0}{V}\right)^{7/3} - \left(\frac{V_0}{V}\right)^{5/3}\right]$$

$$\times \left\{1+\frac{3}{4}(K_0'-4)\left[\left(\frac{V_0}{V}\right)^{2/3}-1\right]\right\},$$

where V is the volume, V_0 is the zero pressure volume, K_0 is the isothermal bulk modulus, and K_0' is the first pressure derivative of the isothermal bulk modulus. By fixing V_0 to be 664.66 Å^3 based on the reported literature we found that the best fit yields $K_0 = 5.8(1)$ GPa and $K_0' = 41.0(3)$ for form-I. For form-III, the fitting results show that $K_0 = 2.8(3)$ GPa and $K_0' = 56.3(8)$.

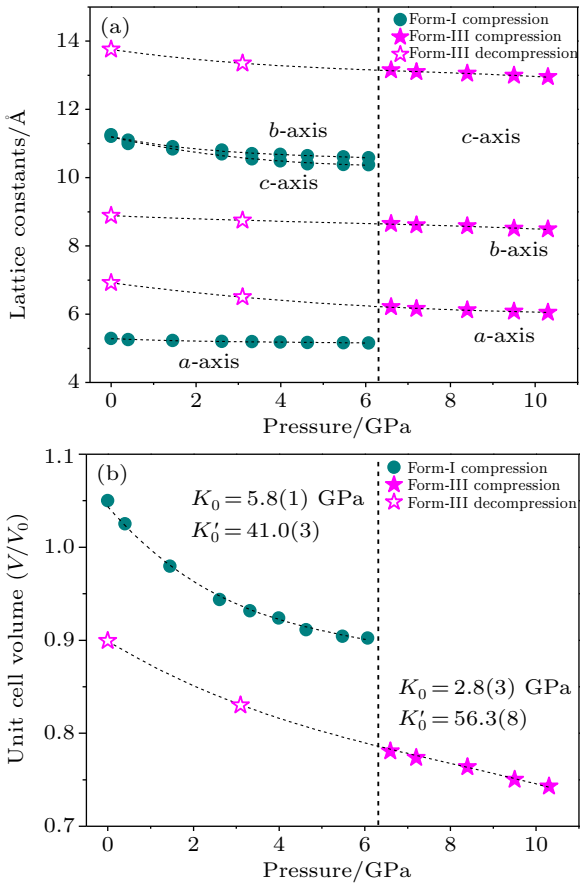


Fig. 7. Compression of (a) lattice constants and (b) unit cell volume of CA with respect to pressure. The vertical dotted line represents the boundary of the two forms.

Figure 7(a) depicts the dependence of lattice constants versus pressure. In form-I, the compression ratios of the three axes are almost the same. This is because CA form-I crystals exhibit three-dimensional structure. Hydrogen bonds are distributed on the three axes of *a*, *b*, and *c*. Each molecule forms four hydrogen bonds in a sort of tetrahedral coordination arrangement to give three-dimensional complex hydrogen-bonded networks. The CA crystal is mainly constructed by these hydrogen bonds. Hydrogen bonds have a certain supporting effect on the pressure. Thus, with the ascending pressure, the *a*-, *b*-, and *c*-axis present small compression ratio. Similarly, CA form-III crystals also possess three-dimensional hydrogen-bonded structure. Therefore, the three axes show almost the same small compression ratio. By contrast to the two-dimensional layered hydrogen-bonded crystals, such as oxamide,[37] maleic hydrazide,[38] and $SnCl_2{\cdot}2H_2O$,[39] three-dimensional hydrogen-bonded crystals have significantly different compression properties. For layered hydrogen-bonded crystals, in the plane in which the hydrogen bonds are located, the compression ratios of the two axes are significantly smaller than the third axis. This is because there is relatively weak van der Waals interaction between the planes only. Consequently, the compression ratio between layers is much larger.

The results of Raman and ADXRD measurements strongly demonstrate the existence of a pressure-induced structural phase transition in CA. On the basis of the experimental results and the proposed crystal structure of form-III, a mechanism for the phase transition was proposed. Figure 8 depicts the comparison of the structures of the two forms. At ambient pressure, hydrogen bonding and van der Waals interactions are the predominant cohesive factors that dominate the stability of CA form-I. The applied pressure continuously reduces the molecular distances. Molecules in the crystals inevitably become closer to one another to achieve close packing. Thus, hydrogen bonding and van der Waals interactions are enhanced. As shown in the Raman spectra, below ~ 6 GPa, as the enhanced hydrogen bonding interaction, modes related to O–H···O, N–H···O, and C–H···O hydrogen bonds exhibit blue shifts. Meanwhile, Gibbs free energy in the system is increased from -12.6263 keV at ambient pressure to -12.6024 keV at 6 GPa, due to the strengthened hydrogen bonding and van der Waals interactions. When the pressure reaches 6.5 GPa, the balance between hydrogen bonding and van der Waals interactions is broken. The hydrogen-bonded networks can no longer support the increased Gibbs free energy. Therefore, reconstructions of hydrogen-bonded networks and phase transition occur to achieve close molecular packing and reduce the total free energy of the system. As shown in Fig. 8, molecules distort and rotate and move away from the original locations to a great extent. Moreover, hydrogen bonds are broken, and new C_4–H_4···O_3=C_7 hydrogen bonds are formed. Meanwhile, various variations of the Raman modes related to O–H···O, N–H···O, and C–H···O hydrogen bonds confirm the reconstructions of hydrogen-bonded networks in CA form-I during phase transition. The experimental and calculated results suggest that hydrogen bonds have a central function in the irreversible structural transition of CA form-I. High-pressure x-ray and neutron diffraction, however, are needed to reliably determine atomic positions in the new polymorph CA form-III.

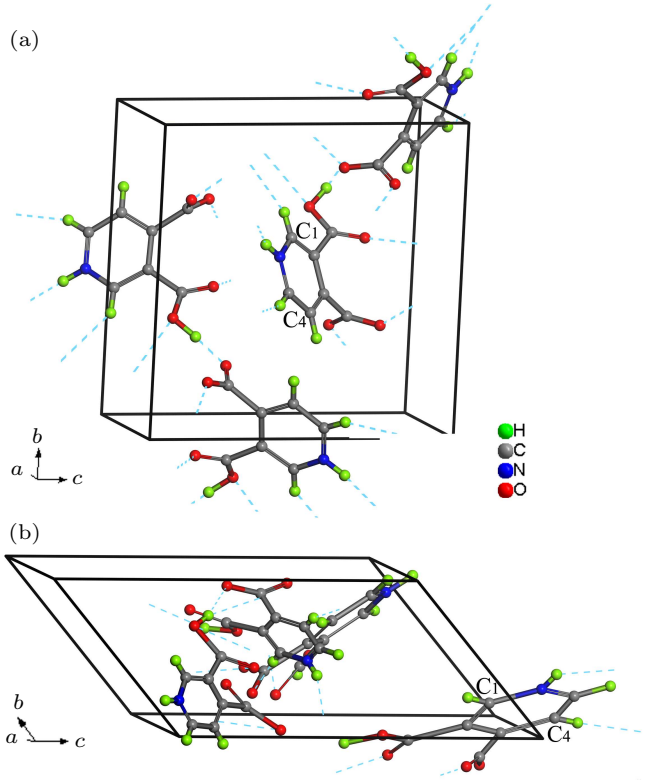


Fig. 8. Comparison of crystal structures of CA: (a) form-I and (b) possible form-III. Hydrogen bonds O–H···O, N–H···O and C–H···O are marked as dashed lines.

4. Conclusion

In summary, we have explored the pressure-induced irreversible phase transition in crystalline CA form-I by virtue of monitoring the evolutions of Raman and ADXRD spectra. The abrupt changes in the spectra at about 6.5 GPa strongly suggested the emergence of a new polymorph, namely CA form-III, which can be retrieved on complete release of pressure. In fact, the pressure of phase transition is usually lower than the observed results. Further analysis indicates that form-III has triclinic $P1$ symmetry. The experimental and calculated results have revealed the phase transition mechanism in terms of the reconstructions of hydrogen-bonded networks and the deformation of the molecular framework. Consequently, this work can be helpful to further understand hydrogen bonds and prepare new polymorphs using a high-pressure technique.

References

[1] McCrone W C 1965 *Physics and Chemistry of the Organic Solid State II*, ed. Fox D, Labes M M and Weissberger A (New York: Interscience) pp. 725–767
[2] Morrow S I 1969 *J. Chem. Educ.* **46** 580
[3] Wöhler F and Liebig J 1832 *Ann. Der Pharm.* **3** 249
[4] David W I, Shankl, K, Pulham C R, Blagden, N, Davey R J and Song M 2005 *Angew. Chem. Int. Ed.* **44** 7032
[5] Gavezzotti A and Filippini G 1995 *J. Am. Chem. Soc.* **117** 12299
[6] Nangia A 2008 *Acc. Chem. Res.* **41** 595
[7] Johnstone R, Lennie A, Parker S, Parsons S, Pidcock E, Richardson P, Warren J and Wood P 2010 *CrystEngComm* **12** 1065
[8] Haleblian J and McCrone W J 1969 *Pharm. Sci.* **58** 911
[9] Yu L, Reutzel S M and Stephenson G A 1998 *Pharm. Sci. Technol. Today* **1** 118
[10] Fabbiani F P A, Allan D R, David W I F, Moggach S A, Parsons S and Pulham C R 2004 *CrystEngComm* **6** 504
[11] Yan T T, Wang K, Duan D F, Tan X, Liu B B and Zou B 2014 *RSC Adv.* **4** 15534
[12] Walker M, Morrison C A, Allan D R, Pulham C R and Marshall W G 2007 *Dalton Trans.* **20** 2014
[13] Yan T T, Xi D Y, Ma Z N, Fan X F and Li Y 2017 *J. Phys. Chem. C* **121** 19365
[14] Allan D R and Clark S J 1999 *Phys. Rev. Lett.* **82** 3464
[15] Yan T T, Xi D Y, Ma Z N, Wang X, Wang Q J and Li Q 2017 *RSC Adv.* **7** 22105
[16] Minkov V S, Goryainov S V, Boldyreva E V and Görbitz C H 2010 *J. Raman Spectrosc.* **41** 1748
[17] Yan T T, Wang K, Tan X, Yang K, Liu B B and Zou B 2014 *J. Phys. Chem. C* **118** 15162
[18] Boldyreva E V, Ahsbahs H, Uchtmann H and Kashcheeva N 2000 *High Press. Res.* **17** 79
[19] Fabbiani F P A and Pulham C R 2006 *Chem. Soc. Rev.* **35** 932
[20] Wang Z and Georgakis C 2017 *Aiche J.* **63** 2796
[21] Okumura T, Ishida M, Takayama K and Otsuka M 2006 *J. Pharm. Sci.* **95** 689
[22] Yan T T, Wang K, Tan X, Liu J, Liu B B and Zou B 2014 *J. Phys. Chem. C* **118** 22960
[23] Laniel D, Downie L E, Smith J S, Savard D, Murugesu M and Desgreniers S 2014 *J. Chem. Phys.* **141** 234506
[24] Griffiths P J 1963 *Acta Crystallogr.* **19** 1074
[25] Takusagawa F, Hirotsu K and Shimada A 1973 *Bull. Chem. Soc. Jpn.* **46** 2669
[26] Braga D, Maini L, Fagnano C, Taddei P, Chierotti M R and Gobettb R 2007 *Chem. Eur. J.* **13** 1222
[27] Karabacak M, Bilgili S and Atac A 2015 *Spectrochim. Acta A* **135** 270
[28] Evans I R, Howard J A K and Evans J S O 2008 *CrystEngComm* **10** 1404
[29] Tong M L, Wang J, Hu S and Batten S R 2005 *Inorg. Chem. Commun.* **8** 48
[30] Senevirathna M K I, Pitigala P, Perera V P S and Tennakone K 2005 *Langmuir* **21** 2997
[31] Errandonea D, Muñoz A and Gonzalez P J 2014 *J. Appl. Phys.* **115** 216101
[32] Chijioke D A, Nellis J W, Soldatov A and Silvera I F 2005 *J. Appl. Phys.* **98** 114905
[33] Park T R, Dreger Z A and Gupta Y M 2004 *J. Phys. Chem. B* **108** 3174
[34] Ciezak J A, Jenkins T A, Liu Z and Hemley R J 2007 *J. Phys. Chem. A* **111** 59
[35] Hamann S D and Linton M 1976 *Aust. J. Chem.* **29** 1641
[36] Lin Y, Ma H W, Matthews C W, Kolb B, Sinogeikin S, Thonhauser T and Mao W L 2012 *J. Phys. Chem. C* **116** 2172
[37] Yan T T, Li S R, Wang K, Tan X, Jiang Z M, Yang K, Liu B B, Zou G T and Zou B 2012 *J. Phys. Chem. B* **116** 9796
[38] Wang K, Liu J, Yang K, Liu B B and Zou B 2014 *J. Phys. Chem. C* **118** 8122
[39] Salinas S R and Nagle J F 1974 *Phys. Rev. B* **9** 4920